HAIT Journal of Science and Engineering A, Volume 5, Issues 1-2, pp. 212-242

Resonance phenomena in macroscopic quantum tunneling: the small viscosity limit *

Yuri N. Ovchinnikov[1], Sara Rombetto[2,*], Berardo Ruggiero[2], Valentina Corato[3], and Paolo Silvestrini[4]

[1] *L.D. Landau Institute for Theoretical Physics, RAS, Moscow, Russia*
[2] *Istituto di Cibernetica "E. Caianiello" del CNR, Pozzuoli, Naples, Italy,*
[3] *ENEA, Frascati, Roma, Italy*
[4] *Dipartimento di Ingegneria dell'Informazione, Seconda Università di Napoli, Naples, Italy*
[*] *Corresponding author: s.rombetto@cib.na.cnr.it*
Received 5 October 2007

Abstract

We present a theoretical study of the resonant quantum behavior for a macroscopic superconducting system interacing with an external microwave at proper frequency. Here we consider a system described by a double well potential, a rf-SQUID, in the extremely underdamped regime. Numerical simulations for resonant phenomena have been performed for this system, whose parameters belong to the range typically used in the experiments. The dependence of the transition probability W on the external drive of the system, φ_x, can show three resonance peaks, in a small microwave frequency range. One peak is connected with the anticrossing and the other two with the external microwave frequency ν. The relative position and the height of the two lateral peaks depends on the microwave frequency. This behavior is studied here for the first time.

PACS: 74.50.+r, 03.65.Yz, 03.67.Lx

*This article was published in Phys. Lett. A, DOI http://dx.doi.org/10.1016/j.physleta.2007.08.061, Yu.N. Ovchinnikov, S. Rombetto, B. Ruggiero, V. Corato, P. Silvestrini, Resonance Phenomena in Macroscopic Quantum Tunneling: the small viscosity limit, Copyright Elsevier (2007).

1 Introduction

Josephson devices are convenient instruments to investigate macroscopic quantum effects [1]. First experiments focused on incoherent phenomena such as macroscopic quantum tunneling (MQT) [2-4] and energy level quantization (ELQ) [5-7]. Recent experiments have shown a coherent superposition of distinct macroscopic quantum states in SQUID systems [8-10] under the action of an external microwave frequency. These results have stimulated many researchers to search for new macroscopic quantum phenomena. Moreover quantum effects in SQUID dynamics are interesting because of possible applications to quantum computing, as demonstrated by recent experiments [11].

The main obstacle in order to observe macroscopic quantum phenomena is the interaction with the environment, since it produces dissipation and it also induces a finite width $\hbar\gamma$ of quantum levels [12] and resonant phenomena can occur only if $\hbar\gamma$ is small compared to the energy difference between levels.

In this paper we study the behavior of a rf-SQUID device, characterized by a double well potential (Fig. 1)in the small viscosity limit, corresponding to $\gamma \ll T_N$ (here T_N is the tunneling frequency) [13], referred as the *extremely underdamped regime*. Up to now, this regime has been investigated for some Josephson devices [7-9,14,15]. In the present paper we focalize on the interaction between a macroscopic quantum system (the rf-SQUID) and an external microwave, for frequencies close to resonant conditions.

The probability of a transition under the potential barrier decreases exponentially by decreasing energy of the quantum state (energy is referred to the bottom of the left potential well). Tunneling can be experimentally observed only if it occurs from a level close to the barrier top and in this case the transition probability, as a function of the external parameter φ_x, can present one or three peaks, as we will show in the following.

A further requirement to observe the quantum tunneling phenomenon is that the number of levels n is not too large, so that no crowding of levels happens. We assume also that the number of levels in the potential well is large enough, so that the motion of a particle with energy close to the top of the potential barrier can be considered quasiclassical. In this limit it is possible to use approximations, as reported in [16]. Moreover in the quasiclassical limit the density of levels close to the barrier top increases, but in the considered case this effect is not significant since numerical factors are of the order of $\frac{1}{2\pi}\ln n$ [16]. Furthermore near to the barrier top, repulsion of levels is relevant and hence the equation for the system wave functions has to

be solved exactly. Finally the tunneling probability of a particle through the potential barrier depends very strongly on the particle energy E and on the energy difference between neighboring levels. The position and the width of each level depends on the external parameters of the system, especially on the φ_x value. A sketch of the double well potential for the rf-SQUID studied here is reported in Fig. 1.

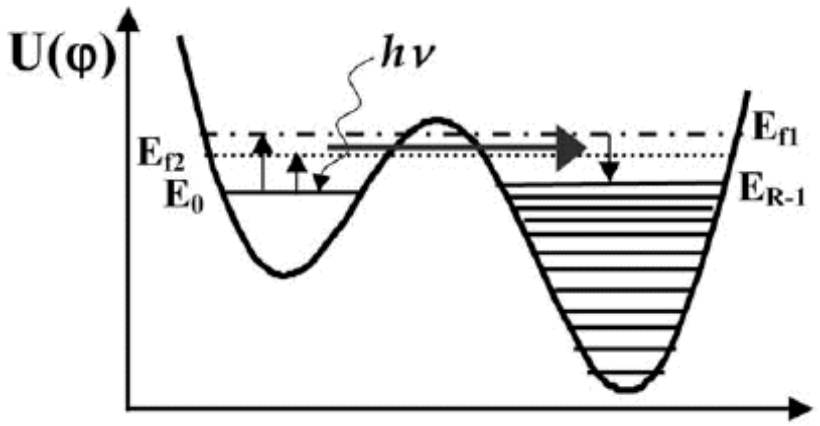

Figure 1: A sketch of an rf-SQUID double-well potential U(φ), with two minima located at φ_1^{min} and φ_2^{min}. φ_{top} is the position of the potential maximum. The coordinates $\varphi_1, \varphi_2, \varphi_3, \varphi_4$ are the "turning points" of energy E_{f_1}. In the same way it is possible to define turning points for energies E_{f_2}, E_0, E_R, E_L. We study the case $E_L = E_0$, that is the ground state in the left potential well.

Out of resonant conditions, energy levels are localized in each well. On the contrary, when two levels in different wells have the same energy, a coherent superposition of distinct states occurs and a gap appears between the energy levels. As a consequence the two levels have an energy tunnel splitting Δ, and the wave functions spread over the two wells, so that two non-degenerate states with energies E_{f_1} and E_{f_2} appear, as shown in Fig. 2.

In order to study the tunneling process from these energy levels, it is necessary to populate them through the application of a microwave of proper frequency $\nu = \omega/2\pi$ and amplitude $\mathcal{I}$, acting on the ground state of the left well. Even a small amplitude of the external microwave frequency can cause an essential change in the population of excited states and therefore can produce a large effect in the tunneling probability.

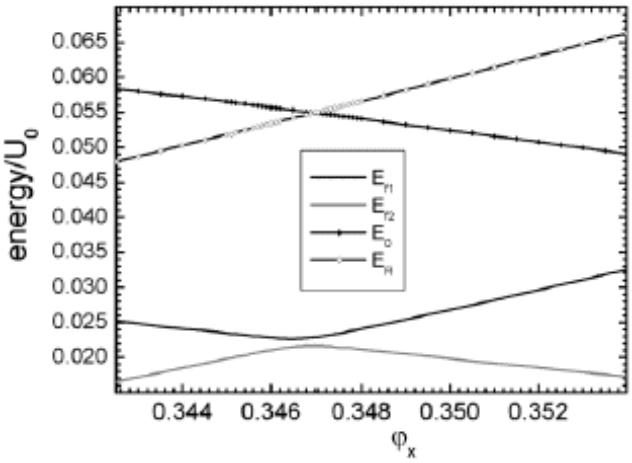

Figure 2: The four essential energy levels considered in this study. All the quantities are referred to the barrier top. Here E_{f_1} and E_{f_2} are the energies of the levels. E_0 is the first level in the left potential well below E_{f_2} and E_R is the first level in the right potential well below E_{f_2}.

We have studied the rf-SQUID dynamics in these particular conditions by the means of numerical calculations. Our study shows that in presence of a microwave the transition probability can present one or three peaks, in the extremely underdamped regime. This effect can be observed only in a small range of microwave frequency and external flux. In these ranges the frequency and the flux should be varied in very small steps in order to have enough resolution. Out of the optimal range or if a too large step is used, only one peak, due to the anticrossing, can be observed. For a fixed value of microwave frequency ν, the transition probability curve W from one potential well to the other one (as a function of the external parameter φ_x) can present three maxima. The three peaks curve is a new prediction. One maximum is connected with the anticrossing, and its position is independent on the external microwave frequency and depends only on the device parameters. The two lateral peaks are due to the interaction of the external microwave frequency with the two levels with energies E_{f_1}, E_{f_2}, and their height and position vary with the ν value.

In the following sections microwave induced resonant phenomena will be discussed by using the density matrix formalism [17].

In Sect. 2 we discuss the transition probability function in the presence of external resonant microwave frequency, in Sect. 3 we show how to calculate levels position and transition matrix elements, in Sect. 4 we determine the energy spectrum in the vicinity of the crossing point and, finally, in Sect. 5 we show the results of numerical calculations for the transition probability W as a function of the external parameter φ_x.

2 Transition probability function in presence of resonant microwave frequency

In the zero approximation for the system interaction with the thermal bath, the hamiltonian describing the rf-SQUID, in the presence of an external microwave with amplitude $\mathcal{I}$ and frequency $\nu = \omega/2\pi$, is

$$H_0 = -\frac{\hbar^2}{2M}\frac{\partial^2}{\partial\varphi^2} + U_0\left[\frac{(\varphi-\varphi_x)^2}{2} + \beta_L\cos\varphi\right] + \frac{\mathcal{I}\hbar}{2e}\cos(\omega t)\varphi \qquad (1)$$

where M is the "mass" of the Josephson junction defined as

$$M = \left(\frac{\hbar}{2e}\right)^2 C \qquad (2)$$

C is the junction capacitance and e is obviously the electron charge. Following a common practice [4], the dimensionless variable φ_x is obtained by referring the magnetic flux to $\Phi_0/2$ and normalizing it to $\Phi_0/2\pi$, where $\Phi_0 = \frac{\pi\hbar}{e}$ is the quantum flux. In Eq. (1) quantities U_0 and β_L are free parameters of the system and are defined as

$$U_0 = \left[\left(\frac{\Phi_0}{2\pi}\right)^2\frac{1}{L}\right] \qquad (3)$$

$$\beta_L = \frac{2\pi L I_c}{\Phi_0} \qquad (4)$$

L and I_c are the inductance and the critical current of the rf-SQUID, respectively. Here we consider the case when U_0 and β_L are constant, while φ_x changes.

Our considerations are valid for any potential $U(\varphi)$ having the form shown in Fig. 1 in the vicinity of the "turning points" φ_i. In this case the frequency of the classical motion in the overturned potential is defined as

$$\Omega_p = \sqrt{\frac{1}{M}\left(\frac{\partial^2 U}{\partial \varphi^2}\right)_{\varphi=\varphi_{min}}} \tag{5}$$

and φ_{min} is the coordinate corresponding to a minimum of the considered potential well. In order to satisfy the conditions for the extremely underdamped regime it should be $\hbar\gamma \ll \hbar\Omega_p$.

We stress that rf-SQUID parameters are such that there are two levels with energies $E_{f_1},\ E_{f_2}$, close to the top of the barrier, that can be considered as belonging to both potential wells simultaneously, as shown in Fig. 1.

In this picture the dissipation is accounted for by the effective resistance R_{eff} defined in the RSJ model for the junction [18]. The R_{eff} accounts for different processes, as a consequence it describes dissipation [3, 18], but it is also related to the quasi-particle tunneling [19, 20], to the normal and the subgap resistance [21]. A bigger R_{eff} implies a better insulation and a smaller width of the levels. Here we consider an rf-SQUID whose Josephson junction presents a large value of resistance R_{eff}, so that the condition

$$\frac{E_{f_1} - E_{f_2}}{\hbar} \gg\ \gamma_1, \gamma_2 \tag{6}$$

is satisfied, where γ_1, γ_2 are the widths of levels having energies $E_{f_1},\ E_{f_2}$ respectively (the exact expression for γ_1, γ_2 is given in the following). Detailed considerations on the processes that lead to the viscosity limit in the Josephson Junction tunnelling dynamics are discussed elsewhere (see refs.[18, 22, 23]). Viscosity can be introduced also with the help of the Hamiltonian (see Eq. (1)) where the "particle" interacts with an infinite number of oscillator, that is the thermal bath (see refs.[1, 13]).

To quantitatively describe the resonant tunneling induced by the external microwave, we use the following system of equations [12] in order to determine the density matrix elements ρ_f^j

$$\begin{aligned}
\frac{\partial \rho_f^j}{\partial t} \;=\; & \frac{i\mathcal{I}}{2e}\cos(\omega t)\sum_m \left(\langle j|\varphi|m\rangle \exp\left[-i\left(\frac{E_m - E_j}{\hbar}\right)t\right]\rho_f^m \right. \\
& \left. -\langle m|\varphi|f\rangle \exp\left[i\left(\frac{E_m - E_f}{\hbar}\right)t\right]\rho_m^j \right) \\
& +\sum_{m,n} W_{f\,n}^{j\,m}\rho_n^m - \frac{1}{2}\sum_m \left(W_{m\,j}^{m\,j} + W_{m\,f}^{m\,f}\right)\rho_f^j
\end{aligned} \tag{7}$$

Here j, m, f, n are the labels for the considered levels, E_j, E_m, E_f, E_n are their energies and t is the time.

The matrix elements $W_{f\,n}^{j\,m}$ entering in Eq. (7) are defined exactly in Appendix A and C. They are nonvanishing provided that

$$|\,(E_m - E_j) - (E_n - E_f)\,| \ll \hbar\Omega_p \tag{8}$$

If this condition is satisfied and the temperature is low enough, the nonvanishing terms $W_{f\,n}^{j\,m}$ of the transition probability matrix have the following expression:

$$\begin{aligned} W_{f\,n}^{j\,m} &= \frac{\pi}{2R_{eff}e^2}\left(1+\tanh\frac{\hbar\tilde{\omega}}{2k_BT}\right)N(\tilde{\omega}) \\ &\cdot\left[\langle j|e^{\frac{i\varphi}{2}}|m\rangle\langle f|e^{-\frac{i\varphi}{2}}|n\rangle + \langle j|e^{-\frac{i\varphi}{2}}|m\rangle\langle f|e^{\frac{i\varphi}{2}}|n\rangle\right] \end{aligned} \tag{9}$$

where

$$\tilde{\omega} = \frac{(E_m - E_j + E_n - E_f)}{2\hbar} \tag{10}$$

and $N\,(\tilde{\omega})$ is defined as

$$N\,(\tilde{\omega}) = \frac{\hbar\tilde{\omega}}{\pi}\coth\left(\frac{\hbar\tilde{\omega}}{2k_BT}\right) \tag{11}$$

where k_B is the Boltzmann constant. We suppose that all eigenfunctions are real. Only the four non-diagonal elements of the density matrix

$$\rho_{f_1}^0,\ \rho_{f_2}^0,\ \rho_0^{f_1},\ \rho_0^{f_2}$$

are nonzero, and they are related by the expressions

$$\rho_0^{f_1} = \left(\rho_{f_1}^0\right)^* \qquad \rho_0^{f_2} = \left(\rho_{f_2}^0\right)^* \tag{12}$$

In the presence of an external microwave frequency also the two diagonal elements $\rho_{f_1}^{f_1}$ and $\rho_{f_2}^{f_2}$ are non-zero.

Here we suppose that the temperature T is such that $k_BT \ll \hbar\Omega_p$ and it is of the order of the energy difference, so that $k_BT \approx (E_{f_1} - E_{f_2})$. Numerical calculations have been performed for $T = 50\,mK$, that is a typical value for our experiments, but it is worth noting that the behavior is the same for all the temperatures that guarantee the sample is in the quantum

regime. If these hypotheses are satisfied, from Eq. (7) we obtain the rate equations

$$\begin{aligned}
\frac{\partial \rho^0_{f_1}}{\partial t} &= -\frac{i\mathcal{I}}{2e}\cos(\omega t)\langle 0|\varphi|f_1\rangle e^{\left(-i\frac{E_{f_1}-E_0}{\hbar}t\right)}\rho^0_0 + W^{0\,0}_{f_1\,f_2}\rho^0_{f_2} - \gamma_1\rho^0_{f_1} \\
\frac{\partial \rho^0_{f_2}}{\partial t} &= -\frac{i\mathcal{I}}{2e}\cos(\omega t)\langle 0|\varphi|f_2\rangle e^{\left(-i\frac{E_{f_2}-E_0}{\hbar}t\right)}\rho^0_0 + W^{0\,0}_{f_2\,f_1}\rho^0_{f_1} - \gamma_2\rho^0_{f_2}
\end{aligned} \tag{13}$$

where the widths γ_1, γ_2 of levels with energies E_{f_1}, E_{f_2} are given by the following expressions

$$\begin{aligned}
\gamma_1 &= \frac{1}{2}\left(W^{f_2\,f_1}_{f_2\,f_1} + W^{L\,f_1}_{L\,f_1} + W^{R\,f_1}_{R\,f_1}\right) \\
\gamma_2 &= \frac{1}{2}\left(W^{f_1\,f_2}_{f_1\,f_2} + W^{L\,f_2}_{L\,f_2} + W^{R\,f_2}_{R\,f_2}\right)
\end{aligned} \tag{14}$$

In order to study the resonant quantum tunneling phenomenon, only five energy levels (E_{f_1}, E_{f_2}, E_0, E_L, E_R) are essential quantities. E_0 is the energy of the ground state in the left potential well, E_L is the first level in the left potential well below E_{f_2}, E_R is the first level in the right potential well below E_{f_2}, and finally E_{f_1} and E_{f_2}. These energy levels vs. the external parameter φ_x, are shown in Fig. 2 (all the energies are referred to E_0). The microwave frequency ν is supposed to be close to the frequencies $E_{f_1}/\hbar$ and $E_{f_2}/\hbar$. Here we have considered the case E_L is also the ground state of the left potential well (E_L=E_0), while in the right well there are many more levels, not involved in the described process. The tunneling transition probability between two states in different wells decreases very quickly for states below the barrier top, such as $e^{-2\pi n}$, where n is the number of states counted from the barrier top [22, 23]. As a consequence it is possible to neglect transitions into lower energy levels in the right potential well.

If these hypotesis are satisfied, the solutions of Eqs. (13) are:

$$\begin{aligned}
\rho^0_{f_1} &= A_{f_1}e^{i\left(\omega-\frac{E_{f_1}-E_0}{\hbar}\right)t} + B_{f_1}e^{i\left(\omega-\frac{E_{f_2}-E_0}{\hbar}\right)t} \\
\rho^0_{f_2} &= B_{f_2}e^{i\left(\omega-\frac{E_{f_1}-E_0}{\hbar}\right)t} + A_{f_2}e^{i\left(\omega-\frac{E_{f_2}-E_0}{\hbar}\right)t}
\end{aligned} \tag{15}$$

where coefficients A_{f_1}, A_{f_2}, B_{f_1}, B_{f_2} are defined as follows

$$
\begin{aligned}
A_{f_1} &= -\frac{\mathcal{I}}{4e}\langle 0|\varphi|f_1\rangle \left[\omega - \frac{E_{f_1}-E_0}{\hbar} - i\gamma_1 + \frac{W^{00}_{f_1 f_2} W^{00}_{f_2 f_1}}{\omega - \frac{E_{f_1}-E_0}{\hbar} - i\gamma_2}\right]^{-1} \\
A_{f_2} &= -\frac{\mathcal{I}}{4e}\langle 0|\varphi|f_2\rangle \left[\omega - \frac{E_{f_2}-E_0}{\hbar} - i\gamma_2 + \frac{W^{00}_{f_1 f_2} W^{00}_{f_2 f_1}}{\omega - \frac{E_{f_2}-E_0}{\hbar} - i\gamma_1}\right]^{-1} \\
B_{f_1} &= -\frac{iW^{00}_{f_1 f_2} A_{f_2}}{\omega - \frac{E_{f_2}-E_0}{\hbar} - i\gamma_1} \\
B_{f_2} &= -\frac{iW^{00}_{f_2 f_1} A_{f_1}}{\omega - \frac{E_{f_1}-E_0}{\hbar} - i\gamma_2}
\end{aligned}
\tag{16}
$$

The diagonal elements $\rho^{f_1}_{f_1}$ and $\rho^{f_2}_{f_2}$ of the density matrix can be found by solving the following rate equations

$$
\begin{aligned}
\frac{\partial \rho^{f_1}_{f_1}}{\partial t} &= \frac{i\mathcal{I}}{2e}\cos(\omega t)\left[\rho^0_{f_1}\langle f_1|\varphi|0\rangle e^{i\left(\frac{E_{f_1}-E_0}{\hbar}\right)t} - \rho^{f_1}_0\langle 0|\varphi|f_1\rangle e^{\left(-i\frac{E_{f_1}-E_0}{\hbar}t\right)}\right] \\
&\quad + W^{f_1 f_2}_{f_1 f_2}\rho^{f_2}_{f_2} - 2\gamma_1\rho^{f_1}_{f_1} \qquad (17) \\
\frac{\partial \rho^{f_2}_{f_2}}{\partial t} &= \frac{i\mathcal{I}}{2e}\cos(\omega t)\left[\rho^0_{f_2}\langle f_2|\varphi|0\rangle e^{i\left(\frac{E_{f_2}-E_0}{\hbar}\right)t} - \rho^{f_2}_0\langle 0|\varphi|f_2\rangle e^{-i\left(\frac{E_{f_2}-E_0}{\hbar}\right)t}\right] \\
&\quad + W^{f_2 f_1}_{f_2 f_1}\rho^{f_1}_{f_1} - 2\gamma_2\rho^{f_2}_{f_2} \qquad (18)
\end{aligned}
$$

Equations 17 and 18 completely describe the dynamics of the process. Their solutions are respectively:

$$
\begin{aligned}
\rho^{f_1}_{f_1}(t) &= \hat{\rho}^{f_1}_{f_1} + \mathcal{F}_1 e^{i\left(\frac{E_{f_2}-E_{f_1}}{\hbar}\right)t} + \mathcal{F}_1^* e^{-i\left(\frac{E_{f_2}-E_{f_1}}{\hbar}\right)t} \qquad (19) \\
\rho^{f_2}_{f_2}(t) &= \hat{\rho}^{f_2}_{f_2} + \mathcal{D}_1 e^{i\left(\frac{E_{f_2}-E_{f_1}}{\hbar}\right)t} + \mathcal{D}_1^* e^{-i\left(\frac{E_{f_2}-E_{f_1}}{\hbar}\right)t} \qquad (20)
\end{aligned}
$$

The expressions for $\mathcal{F}_1$ and $\mathcal{D}_1$ are given in Appendix A, and these coefficients determinate the value of the oscillating part of the tunneling probability W. By substituting Eqs. (19) and (20) inside Eqs. (17) and (18), we obtain the expressions of the quantities $\hat{\rho}^{f_1}_{f_1}$ and $\hat{\rho}^{f_2}_{f_2}$ as following:

$$\hat{\rho}_{f_1}^{f_1} = \frac{\mathcal{I}^2}{16e^2}\frac{1}{\gamma_1\gamma_2 - \frac{1}{4}W_{f_2\,f_1}^{f_2\,f_1}W_{f_1\,f_2}^{f_1\,f_2}} \cdot \Bigg[\gamma_2 \mid \langle 0|\varphi|f_1\rangle \mid^2$$

$$\cdot \frac{\gamma_1 - \gamma_2 W_{f_1\,f_2}^{0\,0}W_{f_2\,f_1}^{0\,0}\left[\left(\omega - \frac{E_{f_1}-E_0}{\hbar}\right)^2 + \gamma_2^2\right]^{-1}}{\left(\omega - \frac{E_{f_1}-E_0}{\hbar}\right)^2 + \gamma_1^2 + \frac{\left(W_{f_1\,f_2}^{0\,0}W_{f_2\,f_1}^{0\,0}\right)^2 + 2W_{f_1\,f_2}^{0\,0}W_{f_2\,f_1}^{0\,0}\left[\left(\omega - \frac{E_{f_1}-E_0}{\hbar}\right)^2 - \gamma_1\gamma_2\right]}{\left(\omega - \frac{E_{f_1}-E_0}{\hbar}\right)^2 + \gamma_2^2}}$$

$$+\frac{1}{2}W_{f_1\,f_2}^{f_1\,f_2} \mid \langle 0|\varphi|f_2\rangle \mid^2$$

$$\cdot \frac{\gamma_2 - \gamma_1 W_{f_1\,f_2}^{0\,0}W_{f_2\,f_1}^{0\,0}\left[\left(\omega - \frac{E_{f_2}-E_0}{\hbar}\right)^2 + \gamma_1^2\right]^{-1}}{\left(\omega - \frac{E_{f_2}-E_0}{\hbar}\right)^2 + \gamma_2^2 + \frac{\left(W_{f_1\,f_2}^{0\,0}W_{f_2\,f_1}^{0\,0}\right)^2 + 2W_{f_1\,f_2}^{0\,0}W_{f_2\,f_1}^{0\,0}\left[\left(\omega - \frac{E_{f_2}-E_0}{\hbar}\right)^2 - \gamma_1\gamma_2\right]}{\left(\omega - \frac{E_{f_2}-E_0}{\hbar}\right)^2 + \gamma_1^2}}\Bigg] \tag{21}$$

$$\hat{\rho}_{f_2}^{f_2} = \frac{\mathcal{I}^2}{16e^2}\frac{1}{\gamma_1\gamma_2 - \frac{1}{4}W_{f_2\,f_1}^{f_2\,f_1}W_{f_1\,f_2}^{f_1\,f_2}} \cdot \Bigg[\gamma_1 \mid \langle 0|\varphi|f_2\rangle \mid^2$$

$$\cdot \frac{\gamma_2 - \gamma_1 W_{f_2\,f_1}^{0\,0}W_{f_1\,f_2}^{0\,0}\left[\left(\omega - \frac{E_{f_2}-E_0}{\hbar}\right)^2 + \gamma_1^2\right]^{-1}}{\left(\omega - \frac{E_{f_2}-E_0}{\hbar}\right)^2 + \gamma_2^2 + \frac{\left(W_{f_1\,f_2}^{0\,0}W_{f_2\,f_1}^{0\,0}\right)^2 + 2W_{f_1\,f_2}^{0\,0}W_{f_2\,f_1}^{0\,0}\left[\left(\omega - \frac{E_{f_2}-E_0}{\hbar}\right)^2 - \gamma_1\gamma_2\right]}{\left(\omega - \frac{E_{f_2}-E_0}{\hbar}\right)^2 + \gamma_1^2}}$$

$$+\frac{1}{2}W_{f_2\,f_1}^{f_2\,f_1} \mid \langle 0|\varphi|f_1\rangle \mid^2$$

$$\cdot \frac{\gamma_1 - \gamma_2 W_{f_1\,f_2}^{0\,0}W_{f_2\,f_1}^{0\,0}\left[\left(\omega - \frac{E_{f_1}-E_0}{\hbar}\right)^2 + \gamma_2^2\right]^{-1}}{\left(\omega - \frac{E_{f_1}-E_0}{\hbar}\right)^2 + \gamma_1^2 + \frac{\left(W_{f_1\,f_2}^{0\,0}W_{f_2\,f_1}^{0\,0}\right)^2 + 2W_{f_1\,f_2}^{0\,0}W_{f_2\,f_1}^{0\,0}\left[\left(\omega - \frac{E_{f_1}-E_0}{\hbar}\right)^2 - \gamma_1\gamma_2\right]}{\left(\omega - \frac{E_{f_1}-E_0}{\hbar}\right)^2 + \gamma_2^2}}\Bigg] \tag{22}$$

It is evident that these two equations are maximized when

$$\omega = \frac{E_{f_1} - E_0}{\hbar} \text{ or } \omega = \frac{E_{f_2} - E_0}{\hbar},$$

that is to say when resonant conditions are satisfied. Now we can introduce the transition probability W from the left to the right potential well. Obviously W is a function of the external parameter φ_x and the final goal of this paper is to compute this quantity. The transition probability is given by the expression

$$W = W_{R\,f_1}^{R\,f_1} \rho_{f_1}^{f_1} + W_{R\,f_2}^{R\,f_2} \rho_{f_2}^{f_2} \tag{23}$$

where, in the low temperature limit, here considered, from Eq. (9) we obtain the expressions

$$W_{R\,f_1}^{R\,f_1} = \frac{2\,(E_{f_1} - E_R)}{R_{eff} e^2} \mid \langle R \mid e^{i\varphi/2} \mid f_1 \rangle \mid^2 \tag{24}$$

$$W_{R\,f_2}^{R\,f_2} = \frac{2\,(E_{f_2} - E_R)}{R_{eff} e^2} \mid \langle R \mid e^{i\varphi/2} \mid f_2 \rangle \mid^2 \tag{25}$$

while the expressions for $\rho_{f_1}^{f_1}$ and $\rho_{f_2}^{f_2}$ are given in Eqs. (19) and (20) respectively.

It is worth noting that any change of the external parameter φ_x leads to a redistribution of wave functions relative to energies E_{f_1}, E_{f_2} between the left and the right potential well, so that transition matrix elements and width of levels are functions of the external parameter φ_x. To complete our considerations we will compute the levels position and the transition matrix elements as a function of the external parameters, as shown in the next section.

3 Levels position and transition matrix elements

As we have seen before, a necessary condition to resolve multiple peaks is that the experimental linewidth of states (γ_1, γ_2) is smaller than Δ ($\Delta \gg \hbar\gamma_1$, $\hbar\gamma_2$). In Fig. 1 $\varphi_1, \varphi_2, \varphi_3, \varphi_4$ are the "turning points", that are the solutions of the following equation

$$U(\varphi_{1,2,3,4}) = E \tag{26}$$

where E is the energy value. In Fig. 1 the points φ_1^{min}, φ_2^{min} are the coordinates corresponding to the minima of potential $U(\varphi)$ and the point φ_{top} is the coordinate corresponding to the maximum of the potential $U(\varphi)$.

For energy values E close to the top of the barrier, the wave function Ψ can be expressed as

$$\Psi = G^{-1} \cdot \frac{1}{\left(2M\left(E - U(\varphi)\right)\right)^{1/4}} \sin\left(\frac{\pi}{4} + \int\limits_{\varphi_1} \sqrt{2M\left(E - U\left(\varphi\right)\right)} d\varphi\right)$$

in the left potential well

$$\begin{aligned} \Psi &= G^{-1} \cdot A \cdot \mathcal{D}_{-\frac{1-i\lambda}{2}}\left((1+i)(2MU_1)^{1/4}(\varphi - \varphi_{top})\right) \\ &\quad + G^{-1} \cdot A^* \mathcal{D}_{-\frac{1+i\lambda}{2}}\left((1-i)(2MU_1)^{1/4}(\varphi - \varphi_{top})\right) \end{aligned} \tag{27}$$

close to the barrier top

$$\Psi = G^{-1} \cdot \frac{B}{\left(2M\left(E - U(\varphi)\right)\right)^{1/4}} \sin\left(\frac{\pi}{4} + \int^{\varphi_4} \sqrt{2M\left(E - U(\varphi)\right)} d\varphi\right)$$

in the right potential well

In Eqs. (27) $\mathcal{D}_p$ is the parabolic cylinder function [24], G is a normalization factor while quantities A and B are numerical factors (they are defined in the following). The other quantities are defined as

$$U_{top} = U(\varphi_{top}) \tag{28}$$

$$U_1 = -\frac{1}{2}\left(\frac{\partial^2 U}{\partial \varphi^2}\right)_{\varphi=\varphi_{top}} \tag{29}$$

$$\lambda = \sqrt{2MU_1}\frac{U_{top} - E}{U_1 \hbar} \tag{30}$$

Near to the top of the potential barrier we use exact solutions of the Schrödinger equation for the considered system, whereas in the vicinity of the points φ_1, φ_4 we use the well known method of outgoing in complex plane [25]. As result the expression for the levels positions is exact and it depends on the parameter λ (that is adimensional). Coefficients A and B, introduced in Eqs. (27), are defined by imposing boundary conditions for these three expressions. By matching coefficients in the right potential well we obtain

$$A = \frac{B}{2^{3/4}(2MU_1)^{1/8}} \cdot \exp\left[\frac{\pi\lambda}{8} - \frac{i\pi}{8} + \frac{i\lambda}{4} + \frac{i\lambda}{4}\ln\left(\frac{2}{\lambda}\right) + i\int\limits_{\varphi_3}^{\varphi_4} d\varphi\sqrt{2M\left(E-U(\varphi)\right)}\right] \tag{31}$$

By matching coefficients in the left potential we obtain two equations. The first one allows to calculate the position of the levels near the barrier top in the case of small viscosity limit

$$\cos\left(\int\limits_{\varphi_3}^{\varphi_4} d\varphi\sqrt{2M\left(E-U(\varphi)\right)} - \int\limits_{\varphi_1}^{\varphi_2} d\varphi\sqrt{2M\left(E-U(\varphi)\right)}\right)$$

$$+ \left(1+\exp(-\pi\lambda)\right)^{1/2}$$

$$\cdot\cos\left(\chi + \tfrac{\lambda}{2} + \tfrac{\lambda}{2}\ln\left(\tfrac{2}{\lambda}\right) + \int\limits_{\varphi_3}^{\varphi_4} d\varphi\sqrt{2M\left(E-U(\varphi)\right)} + \int\limits_{\varphi_1}^{\varphi_2} d\varphi\sqrt{2M\left(E-U(\varphi)\right)}\right)$$

$$= 0 \tag{32}$$

In Eq. (32) phase shift χ is defined by the equation

$$\Gamma\left(\frac{1+i\lambda}{2}\right) = \frac{\sqrt{2\pi}e^{(-\pi\lambda/4)}}{\sqrt{1+e^{(-\pi\lambda)}}}e^{(i\chi)} \tag{33}$$

where $\Gamma(x)$ is the Euler gamma function and the phase χ can be presented in the form

$$\chi = \frac{\lambda}{2}\Psi\left(\frac{1}{2}\right) - \sum_{k=0}^{\infty}\left(\arctan\left(\frac{\lambda}{2k+1}\right) - \frac{\lambda}{2k+1}\right) \tag{34}$$

In Eq. (34) $\psi(x)$ is the Euler function and

$$\psi\left(\frac{1}{2}\right) = -C - 2\ln 2 = -1.96351 \tag{35}$$

The second equation allows to calculate the value of the coefficient B as follows

$$B = \exp\left(\tfrac{\pi\lambda}{2}\right)\Bigg[\left(1+\exp\left(-\pi\lambda\right)\right)^{1/2}$$

$$\cdot\sin\left(\chi+\tfrac{\lambda}{2}+\tfrac{\lambda}{2}\ln\left(\tfrac{2}{\lambda}\right)+\int\limits_{\varphi_1}^{\varphi_2}d\varphi\sqrt{2M\left(E-U(\varphi)\right)}+\int\limits_{\varphi_3}^{\varphi_4}d\varphi\sqrt{2M\left(E-U(\varphi)\right)}\right)$$

$$-\sin\left(\int\limits_{\varphi_1}^{\varphi_2}d\varphi\sqrt{2M\left(E-U(\varphi)\right)}-\int\limits_{\varphi_3}^{\varphi_4}d\varphi\sqrt{2M\left(E-U(\varphi)\right)}\right)\Bigg] \tag{36}$$

In order to obtain two non-degenerate levels (E_{f_1}, E_{f_2}) close to the barrier top the parameter λ should be $\lambda \geq 1$. In such a case, the normalization factor G can be approximated as

$$G^2 = \frac{\hbar}{2}\left(\int\limits_{\varphi_1}^{\varphi_2}\frac{d\varphi}{\sqrt{2M\left(E-U(\varphi)\right)}}+B^2\int\limits_{\varphi_3}^{\varphi_4}\frac{d\varphi}{\sqrt{2M\left(E-U(\varphi)\right)}}\right) \tag{37}$$

Moreover, since we consider the case the energy E is close to the barrier top, it is possible to use expressions with an explicit energy dependence (by using perturbation theory over the quantity $(U_{top}-E)$ with separation of the singular terms):

$$\int_{\varphi_1}^{\varphi_2}d\varphi\sqrt{2M\left(E-U(\varphi)\right)}=\int_{\tilde{\varphi}_1}^{\varphi_{top}}d\varphi\sqrt{2M\left(U_{top}-U(\varphi)\right)}$$

$$-\left(U_{top}-E\right)\sqrt{\tfrac{M}{2}}\int_{\tilde{\varphi}_1}^{\varphi_{top}}d\varphi\left(\frac{1}{\sqrt{\left(U_{top}-U(\varphi)\right)}}-\frac{\sqrt{\varphi_{top}-\tilde{\varphi}_1}}{\left(\varphi_{top}-\varphi\right)\sqrt{U_1(\varphi-\tilde{\varphi}_1)}}\right) \tag{38}$$

$$-\left(U_{top}-E\right)\sqrt{\tfrac{M}{2U_1}}\left[\ln\left(\frac{8\left(\varphi_{top}-\tilde{\varphi}_1\right)\sqrt{U_1}}{\sqrt{U_{top}-E}}\right)+\tfrac{1}{2}\right]$$

$$\int_{\varphi_3}^{\varphi_4}d\varphi\sqrt{2M\left(E-U(\varphi)\right)}=\int_{\varphi_{top}}^{\tilde{\varphi}_4}d\varphi\sqrt{2M\left(U_{top}-U(\varphi)\right)}$$

$$-\left(U_{top}-E\right)\sqrt{\tfrac{M}{2}}\int_{\varphi_{top}}^{\tilde{\varphi}_4}d\varphi\left(\frac{1}{\sqrt{\left(U_{top}-U(\varphi)\right)}}-\frac{\sqrt{\tilde{\varphi}_4-\varphi_{top}}}{\left(\varphi-\varphi_{top}\right)\sqrt{U_1(\tilde{\varphi}_4-\varphi)}}\right) \tag{39}$$

$$-\left(U_{top}-E\right)\sqrt{\tfrac{M}{2U_1}}\left[\ln\left(\frac{8\left(\tilde{\varphi}_4-\varphi_{top}\right)\sqrt{U_1}}{\sqrt{U_{top}-E}}\right)+\tfrac{1}{2}\right]$$

In Eqs. (38), (39) quantities $\tilde{\varphi}_1$, $\tilde{\varphi}_4$ are defined as

$$\begin{aligned} \tilde{\varphi}_1 &= \varphi_1 \ (E = U_{top}) \\ \tilde{\varphi}_4 &= \varphi_4 \ (E = U_{top}) \end{aligned}$$

Energies E_L, E_R of states Ψ_L, Ψ_R (defined in Sect. 2) can be found by using Eqs. (32), (38), (39), provided that Ψ_L, Ψ_R are referred to the barrier top. In this case wavefunctions Ψ_L, Ψ_R can be described by using the quasiclassical approximation, so that we find

$$\Psi_L = \frac{1}{G_L} \frac{\sin\left(\frac{\pi}{4} + \int\limits_{\varphi_1}^{\varphi} d\varphi \sqrt{2M\left(E - U(\varphi)\right)}\right)}{\left(2M\left(E - U(\varphi)\right)\right)^{1/4}} \tag{40}$$

$$\Psi_R = \frac{1}{G_R} \frac{\sin\left(\frac{\pi}{4} + \int\limits_{\varphi}^{\varphi_4} d\varphi \sqrt{2M\left(E - U(\varphi)\right)}\right)}{\left(2M\left(E - U(\varphi)\right)\right)^{1/4}} \tag{41}$$

where the factors G_L and G_R are

$$G_L^2 = \frac{\hbar}{2} \int\limits_{\varphi_1}^{\varphi_2} \frac{d\varphi}{\sqrt{2M\left(E - U(\varphi)\right)}} \tag{42}$$

$$G_R^2 = \frac{\hbar}{2} \int\limits_{\varphi_3}^{\varphi_4} \frac{d\varphi}{\sqrt{2M\left(E - U(\varphi)\right)}} \tag{43}$$

Finally the wave function Ψ_0 of the ground state can be taken in the form

$$\Psi_0 = \frac{\left(2MU_1^{min}\right)^{1/8}}{\pi^{1/4}} \, e^{\left(-\int\limits_{\varphi_1^{min}}^{\varphi} d\varphi \sqrt{2M\left(U(\varphi) - U(\varphi_1^{min})\right)}\right)} \tag{44}$$

where $U_{1,2}^{min} = U(\varphi_{1,2}^{min})$ and $\varphi_{1,2}^{min}$ are the coordinates corresponding to the position of the left and right minimum in the potential $U(\varphi)$

$$\begin{aligned} \left(\frac{\partial U}{\partial \varphi}\right)_{\varphi = \varphi_{1,2}^{min}} &= 0 \\ U(\varphi) &= U(\varphi_{1,2}^{min}) + U_{1,2}^{min}(\varphi - \varphi_{1,2}^{min})^2 + ... \end{aligned}$$

4 The energy spectrum in the vicinity of the crossing point

In order to better describe the energy spectrum near to the crossing point we introduce the functions Φ_1 and Φ_2, defined as:

$$\begin{aligned}
\Phi_1 &= \int_{\varphi_1}^{\varphi_2} d\varphi \sqrt{2M\left(E-U(\varphi)\right)} + \frac{\lambda}{4}\left(1+\ln\left(\frac{2}{\lambda}\right)\right) \\
&= \int_{\tilde{\varphi}_1}^{\varphi_{top}} d\varphi \sqrt{2M\left(U_{top}-U(\varphi)\right)} - \left(U_{top}-E\right)\sqrt{\frac{M}{2}} \qquad (45) \\
&\quad \cdot \int_{\tilde{\varphi}_1}^{\varphi_{top}} d\varphi \left(\frac{1}{\sqrt{U_{top}-U(\varphi)}} - \frac{\sqrt{\varphi_{top}-\tilde{\varphi}_1}}{\left(\varphi_{top}-\varphi\right)\left(\sqrt{U_1\left(\varphi-\tilde{\varphi}_1\right)}\right)}\right) \\
&\quad + \left(U_{top}-E\right)\sqrt{\frac{M}{2U_1}}\ln\left(\frac{2^{1/4}}{8\left(MU_1\right)^{1/4}\left(\varphi_{top}-\tilde{\varphi}_1\right)}\right)
\end{aligned}$$

$$\begin{aligned}
\Phi_2 &= \int_{\varphi_3}^{\varphi_4} d\varphi \sqrt{2M\left(E-U(\varphi)\right)} + \frac{\lambda}{4}\left(1+\ln\left(\frac{2}{\lambda}\right)\right) \\
&= \int_{\varphi_{top}}^{\tilde{\varphi}_4} d\varphi \sqrt{2M\left(U_{top}-U(\varphi)\right)} - \left(U_{top}-E\right)\sqrt{\frac{M}{2}} \qquad (46) \\
&\quad \cdot \int_{\varphi_{top}}^{\tilde{\varphi}_4} d\varphi \left(\frac{1}{\sqrt{U_{top}-U(\varphi)}} - \frac{\sqrt{\tilde{\varphi}_4-\varphi_{top}}}{\left(\varphi-\varphi_{top}\right)\left(\sqrt{U_1\left(\tilde{\varphi}_4-\varphi\right)}\right)}\right) \\
&\quad + \left(U_{top}-E\right)\sqrt{\frac{M}{2U_1}}\ln\left(\frac{2^{1/4}}{8\left(MU_1\right)^{1/4}\left(\tilde{\varphi}_4-\varphi_{top}\right)}\right)
\end{aligned}$$

Now we suppose that for some value of the external parameters φ_x^0, U_0, β_L there is a point characterized by E_0, $\lambda_0 = \lambda\left(E_0\right)$ (defined in Eq. 30) such that

$$\Phi_1\left(U_0,\beta_L,\varphi_x^0,E_0,\lambda_0\right) + \frac{1}{2}\chi\left(\lambda_0\right) = \frac{\pi}{2}+\pi k_1 \qquad (47)$$

$$\Phi_2\left(U_0,\beta_L,\varphi_x^0,E_0,\lambda_0\right) + \frac{1}{2}\chi\left(\lambda_0\right) = \frac{\pi}{2}+\pi k_2 \qquad (48)$$

where k_1, k_2 are integer numbers. Equations (45), (46) allow to determine the external parameter φ_x such that the two energy levels E_{f1} and E_{f2} are closest. Next to this special point, it is possible to use Taylor expansion for the functions Φ_1 and Φ_2 and we can write:

$$\Phi_1 + \frac{1}{2}\chi = \frac{\pi}{2} + \pi k_1 + \alpha_1 \delta\varphi_x + \beta_1 \delta E \tag{49}$$

$$\Phi_2 + \frac{1}{2}\chi = \frac{\pi}{2} + \pi k_2 + \alpha_2 \delta\varphi_x + \beta_2 \delta E \tag{50}$$

where

$$E = E_0 + \delta E, \quad \varphi_x = \varphi_x^0 + \delta\varphi_x \tag{51}$$

and the quantities α_1, α_2, β_1, β_2 are given in Appendix B.

From Eqs. (32), (49), (50) we obtain the equation to calculate the energy spectrum for two close levels near to the barrier top

$$\beta_1\beta_2(\delta E)^2 + \alpha_1\alpha_2(\delta\varphi_x)^2 + (\alpha_1\beta_2 + \alpha_2\beta_1)\delta\varphi_x\delta E - \frac{1}{4}e^{(-\pi\lambda)} = 0 \tag{52}$$

The solutions of this equation are two hyperboles, as shown in Fig. 3

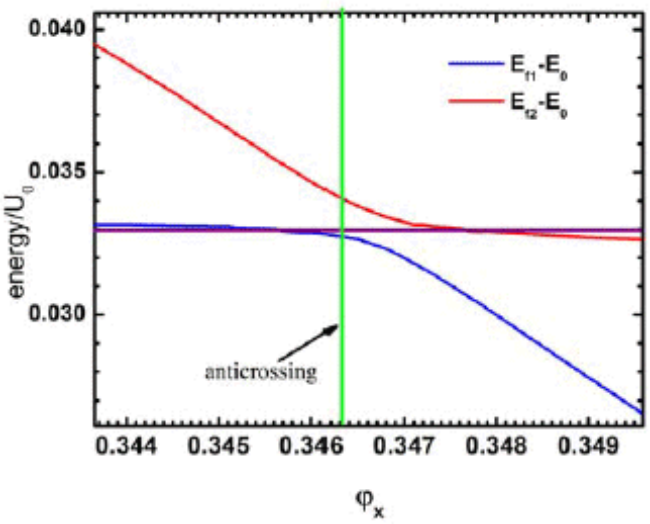

Figure 3: Curves $E_{f_1} - E_0$ vs. φ_x and $E_{f_2} - E_0$ vs. φ_x obtained by solving Eq. (32). All the energies are referred to the barrier top. The horizontal line is the external field of frequency ν, it crosses the energy curves E_{f_1}-E_0 and E_{f_2}-E_0 in two points. The vertical line represents the coordinate corresponding to the anticrossing point. For all the parameters values are: $\beta_L = 1.75$, $C = 0.1\,pF$, $L = 210\,pH$.

$$\delta E = -\frac{1}{2\beta_1\beta_2} \cdot \left[(\alpha_1\beta_2 + \alpha_2\beta_1)\delta\varphi_x \pm \sqrt{(\alpha_1\beta_2 - \alpha_2\beta_1)^2(\delta\varphi_x)^2 + \beta_1\beta_2\exp(-\pi\lambda)}\right] \tag{53}$$

Note that Eq.(53) gives the position of two close levels as a function of the external parameter φ_x for any λ value. If we consider the case λ is a real parameter in the Eq. (53), hence the splitting of energy levels is small if we consider the case $\lambda > 1$. For λ=1 from Eq. (30) we obtain

$$\frac{U_{top} - E}{\hbar\Omega_p} = \frac{1}{2} \tag{54}$$

The two levels having energies E_{f_1}, E_{f_2} have to satisfy the condition $\delta E \ll \hbar\Omega_p$ and this occurs if the parameter $\exp(-\pi\lambda)$ is small, that is true if λ is of the order of one, so that $\exp(-\pi\lambda)$ is of the order of 10^{-2}.

5 Numerical calculations

As we have said before, these resonant quantum effects can be experimentally observed only in a small frequency range and for a device realized with proper parameters. In this section we suggest a set of rf-SQUID parameters useful in order to experimentally observe the effect studied here.

For the calculations presented here we consider a temperature T=50 mK and the following rf-SQUID parameters: β_L=1.75, L=210 pH, C=0.1 pF. Finally we consider the effective resistance R_{eff}=8 MΩ.

In the extremely underdamped limit, the number of peaks of the transition probability W vs. φ_x, can be three or one depending on the microwave frequency value ν.

It is possible to observe a three peaks curve (see Fig. 4) only in a small range of frequency and external flux. Moreover it is necessary to use small steps in order to have a good resolution. This is possible because we are considering the case the levels are well defined. In this case, one peak (the central one) is connected with the anticrossing, while the other two peaks are due to the interaction of the microwave frequency with levels f_1, f_2. As a consequence, the central peak is fixed in position and height, even if we change the frequency ν, since the anticrossing does not depend on the external microwave frequency ν. On the contrary, the other two peaks have a shift depending on the frequency. Of course transitions described by these

peaks occur at values of the external flux φ_x which depend on the microwave frequency, as shown in Fig. 3. If we represent the external microwave having frequency ν with a horizontal line, it is possible to obtain the three peaks curve only when the frequency crosses both the energy curves E_{f_1}-E_0 and E_{f_2}-E_0. This condition has to be satisfied also in the moderate underdamped regime [26], but in the considered case the levels have a better resolution since their width is really small.

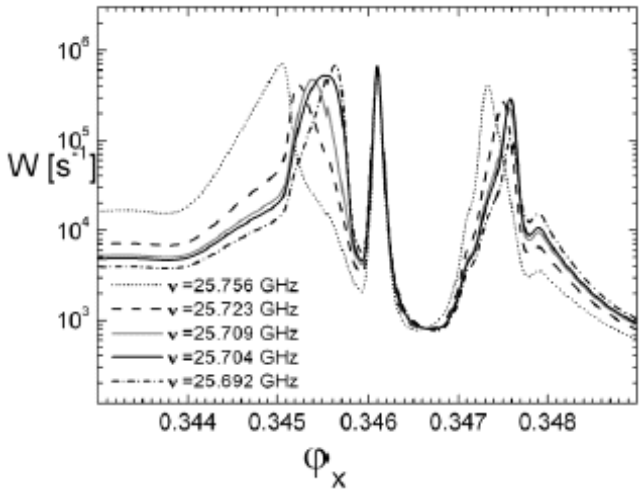

Figure 4: Transition probability W vs. φ_x for different values of the external microwave frequency ν. W presents three peaks: the central one is due to the anticrossing and two lateral ones are due to the microwave frequency interacting with the two levels close to the barrier top. Curves are obtained by using the following parameters for the numerical calculations: β_L=1.75, L=210 pH, C=0.1 pF, and R_{eff}=8 MΩ.

For calculations presented in this paper we have considered microwave frequencies ranging from $\nu = \omega/2\pi$ = 25.76 GHz to ν =26.69 GHz to obtain three peaks curves. For frequencies not belonging to this interval, the transition probability is a one peak curve (Fig. 5). The only peak is due to the anticrossing and does not depend on microwave frequency, so it is fixed in height and position.

Moreover we have studied the dependence of the peaks on the effective dissipation described in the RSJ model by the effective resistance R_{eff}. As expected [27], by increasing R_{eff}, peaks resolution is enhanced (Fig. 6).

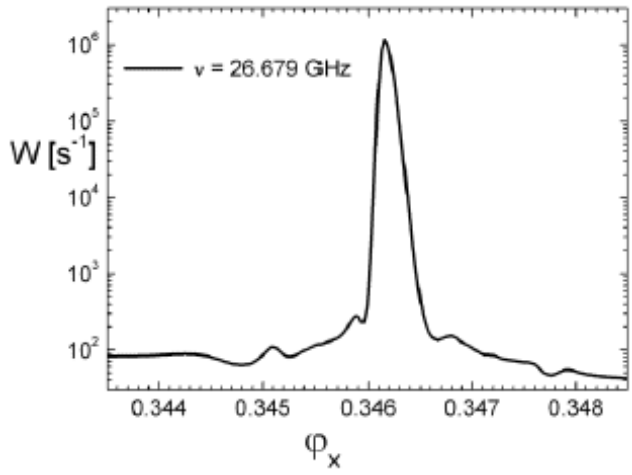

Figure 5: Transition probability W vs. φ_x. Here the W presents only one peak due to the anticrossing. The plot was obtained by using the following parameters for the numerical calculations: β_L=1.75, L=210 pH, C=0.1 pF, and R_{eff}=8 MΩ.

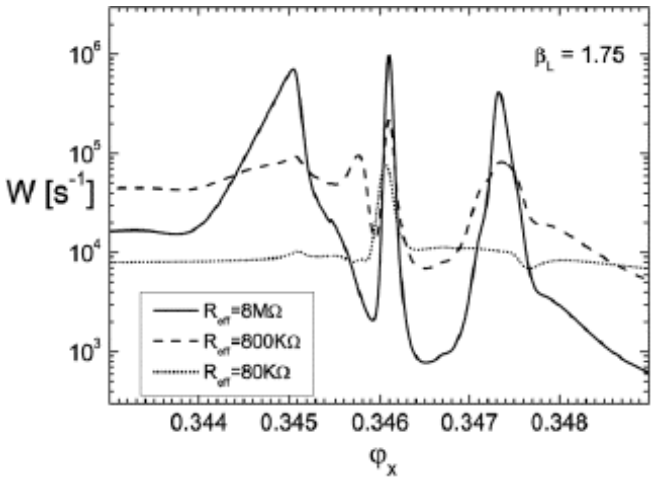

Figure 6: Transition probability W vs. φ_x for different values of the effective resistance R_{eff}. The plot was obtained by using the following parameters for the numerical calculations: β_L=1.75, L=210 pH, C=0.1 pF, ν= 25.756 GHz.

It is possible to observe that the width of central peak is fixed while the lateral peaks width changes. This is due to the change in level position for different R_{eff} values.

Also the β_L parameter can be varied in the experiments [8] and therefore we present some numerical calculations to study the transition probability W vs.φ_x for three different β_L values (see Fig. 7, Fig. 8 and Fig. 9). It is worth noting that the variation of β_L, corresponding to a variation of the rf-SQUID potential barrier height, here has been obtained by changing only the value of the inductance L (see Eq. 3), while I_c has been kept constant. We have observed that, when we increase the β_L value, the transition probability becomes smaller so that it is necessary to increase the φ_x value to observe the peaks. Again, it is possible to observe that the width of central peak is fixed while the lateral peaks width changes.

Calculations we have made suggest to choose a Josephson system with a small capacitance and a β_L not too large, but definitely greater than 1. The set of parameters used here seems to be a good compromise to achieve the experimental observation of the phenomenon.

The experiment can be realized by using the experimental set-up described in [7] and measuring the statistical distribution of the switching value φ_x can be measured by repeating the process many times (about 10^4). From the switching value distribution is straightforward to obtain the escape rate W and to compare data and theory.

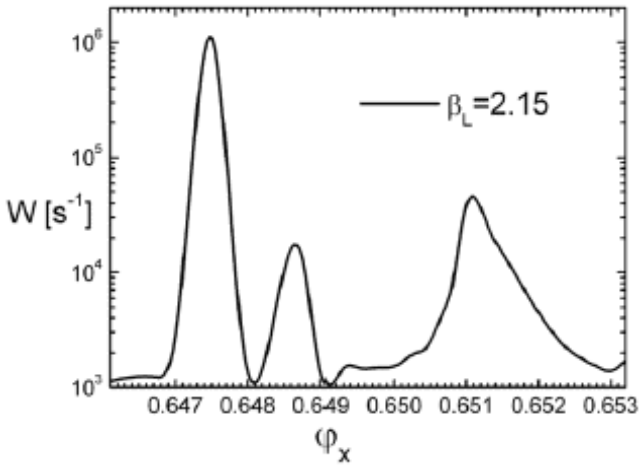

Figure 7: Transition probability W vs. φ_x for β_L=2.15, L=258 pH, C=0.1 pF, R_{eff}=8 MΩ and ν=32.818 GHz.

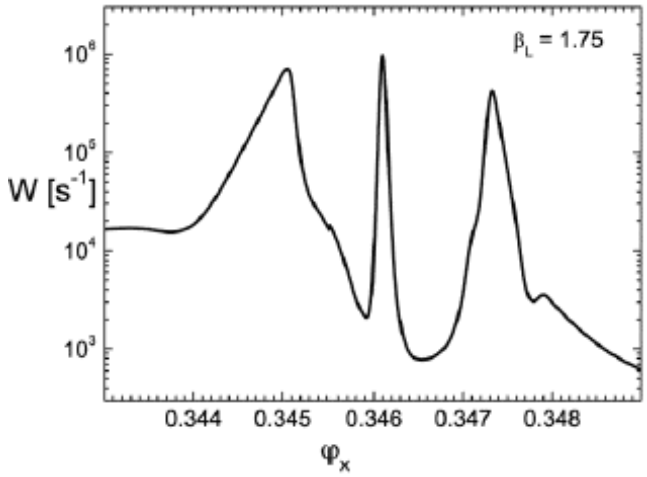

Figure 8: Transition probability W vs. φ_x for β_L=1.75, L=210 pH, C=0.1 pF, R_{eff}=8 MΩ and ν= 25.756 GHz.

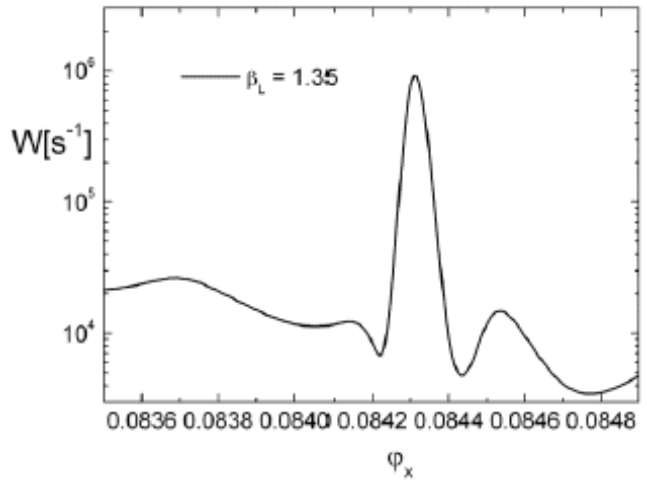

Figure 9: Transition probability W vs. φ_x for β_L=1.35, L=162 pH, C=0.1 pF, R_{eff}=8 MΩ and ν= 24.456 GHz.

6 Conclusions

Results presented here describe the small viscosity limit for the resonant quantum tunneling for an rf-SQUID, realized with proper parameters. No fitting parameters have been used to obtain the following physical quantities: levels position, width of levels, transition probability W from the left to the right well. These quantities are expressed as a function of the external parameters (like junction capacitance, external current, microwave frequency and amplitude). It is worth noting that levels essential to study this phenomenon are placed below the top of the barrier and that the distance between them is of the order of $\hbar\Omega_p$. The level splitting should be such that to satisfy two essential conditions: it should be much smaller than $\hbar\Omega_p$ and at the same time it should be large enough to be experimentally observed.

The transition probability W from the left to the right potential well has been calculated as a function of the external parameters (they are φ_x, the microwave frequency ν, the effective resistance R_{eff}, β_L). Results obtained here suggest that the resonant quantum tunneling is a convenient tool to investigate macroscopic quantum phenomena.

Our study shows that in resonant conditions and in presence of a proper microwave frequency the transition probability W vs. external parameter φ_x can show three peaks (Fig. 4). The first is connected with the anticrossing and the other two are due to the interaction of the microwave frequency with the two energy levels E_{f_1}, E_{f_2}. The relative positions of these two peaks strictly depend on the microwave frequency and on the external parameter biasing the rf-SQUID and they disappear for frequency values external to this small range.

Appendix A

In this appendix we give the explicit expression of quantities $\mathcal{D}_1$ and $\mathcal{F}_1$, which appear in Eqs. (19), (20) as well as of the matrix elements $W_{f\,n}^{j\,m}$ entering in Eq. (7).

Inserting Eqs. (19, 20) into Eqs. (17), (18) we obtain two equations depending on the quantities $\mathcal{D}_1$ and $\mathcal{F}_1$

$$\mathcal{F}_1\left[\left(\tfrac{E_{f_2}-E_{f_1}}{\hbar}\right)-2i\gamma_1\right]+iW^{f_1\,f_2}_{f_1\,f_2}\mathcal{D}_1=$$

$$\tfrac{i\mathcal{I}^2}{16e^2}\cdot\left[\frac{\langle 0|\varphi|f_1\rangle\langle f_2|\varphi|0\rangle W^{0\;0}_{f_1\,f_2}}{\left(\omega-\left(\tfrac{E_{f_2}-E_0}{\hbar}\right)\right)^2-\gamma_1\gamma_2+W^{0\;0}_{f_1\,f_2}W^{0\;0}_{f_2\,f_1}+i(\gamma_1+\gamma_2)\left(\omega-\left(\tfrac{E_{f_2}-E_0}{\hbar}\right)\right)}\right] \tag{A.1}$$

$$iW^{f_2\,f_1}_{f_2\,f_1}\mathcal{F}_1+\mathcal{D}_1\left[\left(\tfrac{E_{f_2}-E_{f_1}}{\hbar}\right)-2i\gamma_2\right]=$$

$$\tfrac{i\mathcal{I}^2}{16e^2}\cdot\left[\frac{\langle 0|\varphi|f_1\rangle\langle f_2|\varphi|0\rangle W^{0\;0}_{f_2\,f_1}}{\left(\omega-\left(\tfrac{E_{f_1}-E_0}{\hbar}\right)\right)^2-\gamma_1\gamma_2+W^{0\;0}_{f_1\,f_2}W^{0\;0}_{f_2\,f_1}-i(\gamma_1+\gamma_2)\left(\omega-\left(\tfrac{E_{f_1}-E_0}{\hbar}\right)\right)}\right] \tag{A.2}$$

Solution of equations (A.1) is

$$\mathcal{F}_1=\tfrac{i\mathcal{I}^2}{16e^2}\cdot\frac{\langle 0|\varphi|f_1\rangle\langle f_2|\varphi|0\rangle}{\left(\tfrac{E_{f_2}-E_{f_1}}{\hbar}\right)^2-4\gamma_1\gamma_2-2i(\gamma_1+\gamma_2)\left(\tfrac{E_{f_2}-E_{f_1}}{\hbar}\right)+W^{f_1\,f_2}_{f_1\,f_2}W^{f_2\,f_1}_{f_2\,f_1}}\cdot$$

$$\cdot\left[\frac{\left[\tfrac{E_{f_2}-E_{f_1}}{\hbar}-2i\gamma_2\right]W^{0\;0}_{f_1\,f_2}}{\left(\omega-\tfrac{E_{f_2}-E_0}{\hbar}\right)^2-\gamma_1\gamma_2+W^{0\;0}_{f_1\,f_2}W^{0\;0}_{f_2\,f_1}+i(\gamma_1+\gamma_2)\left(\omega-\tfrac{E_{f_2}-E_0}{\hbar}\right)}\right. \tag{A.3}$$

$$\left.-i\frac{W^{f_1\,f_2}_{f_1\,f_2}W^{0\;0}_{f_2\,f_1}}{\left(\omega-\tfrac{E_{f_1}-E_0}{\hbar}\right)^2-\gamma_1\gamma_2+W^{0\;0}_{f_1\,f_2}W^{0\;0}_{f_2\,f_1}-i(\gamma_1+\gamma_2)\left(\omega-\tfrac{E_{f_1}-E_0}{\hbar}\right)}\right]$$

$$\mathcal{D}_1=\tfrac{i\mathcal{I}^2}{16e^2}\cdot\frac{\langle 0|\varphi|f_1\rangle\langle f_2|\varphi|0\rangle}{\left(\tfrac{E_{f_2}-E_{f_1}}{\hbar}\right)^2-4\gamma_1\gamma_2-2i(\gamma_1+\gamma_2)\tfrac{E_{f_2}-E_{f_1}}{\hbar}+W^{f_1\,f_2}_{f_1\,f_2}W^{f_2\,f_1}_{f_2\,f_1}}\cdot$$

$$\left[\frac{\left[\tfrac{E_{f_2}-E_{f_1}}{\hbar}-2i\gamma_1\right]W^{0\;0}_{f_2\,f_1}}{\left(\omega-\tfrac{E_{f_1}-E_0}{\hbar}\right)^2-\gamma_1\gamma_2+W^{0\;0}_{f_1\,f_2}W^{0\;0}_{f_2\,f_1}-i(\gamma_1+\gamma_2)\left(\omega-\tfrac{E_{f_1}-E_0}{\hbar}\right)}\right. \tag{A.4}$$

$$\left.-i\frac{W^{f_2\,f_1}_{f_2\,f_1}W^{0\;0}_{f_1\,f_2}}{\left(\omega-\tfrac{E_{f_2}-E_0}{\hbar}\right)^2-\gamma_1\gamma_2+W^{0\;0}_{f_1\,f_2}W^{0\;0}_{f_2\,f_1}+i(\gamma_1+\gamma_2)\left(\omega-\tfrac{E_{f_2}-E_0}{\hbar}\right)}\right]$$

The explicit expression for the transition matrix elements $W^{f_1\,f_2}_{f_1\,f_2}$ and $W^{0\;0}_{f_1\,f_2}$ is given below

$$\begin{aligned} W^{f_1\,f_2}_{f_1\,f_2} &= \frac{\pi}{R_{eff}e^2}\left(1+\tanh\left(\frac{E_{f_2}-E_{f_1}}{2k_BT}\right)\right)\frac{E_{f_2}-E_{f_1}}{\pi} \\ &\quad \cdot\coth\left(\frac{E_{f_2}-E_{f_1}}{2k_BT}\right)|\langle f_1|\exp^{i\frac{\varphi}{2}}|f_2\rangle|^2 \end{aligned} \tag{A.5}$$

$$\begin{aligned} W^{0\;0}_{f_1\,f_2} &= \frac{\pi}{2R_{eff}e^2}\left(1+\tanh\left(\frac{E_{f_2}-E_{f_1}}{4k_BT}\right)\right)\frac{E_{f_2}-E_{f_1}}{2\pi}\coth\left(\frac{E_{f_2}-E_{f_1}}{4k_BT}\right) \\ &\quad \cdot\left[\langle 0|\exp^{i\frac{\varphi}{2}}|0\rangle\langle f_1|\exp^{-i\frac{\varphi}{2}}|f_2\rangle+\langle 0|\exp^{-i\frac{\varphi}{2}}|0\rangle\langle f_1|\exp^{i\frac{\varphi}{2}}|f_2\rangle\right] \end{aligned} \tag{55}$$

$$W^{0\;0}_{f_2\,f_1} = \exp\left(-\frac{E_{f_2}-E_{f_1}}{2k_BT}\right)W^{0\;0}_{f_1\,f_2} \tag{A.7}$$

Appendix B

In this appendix explicit expression of quantities α_1, α_2, β_1 and β_2, appearing in Eqs. (49) and (50) are given. For the potential, given by Eq. (1) we have

$$\begin{aligned} \varphi_{top} &= \varphi_x+\beta_L\sin(\varphi_{top}) \\ \frac{\partial\varphi_{top}}{\partial\varphi_x} &= -\frac{1}{\beta_L\cos(\varphi_{top})-1} \\ \frac{\partial U}{\partial\varphi_x} &= -U_0(\varphi-\varphi_x) \end{aligned}$$

$$\begin{aligned} U_1 &= \frac{U_0}{2}\left(\beta_L\cos(\varphi_{top})-1\right) \\ \frac{\partial U_1}{\partial\varphi_x} &= \frac{1}{2}\beta_L U_0\frac{\sin(\varphi_{top})}{\beta_L\cos(\varphi_{top})-1} \end{aligned}$$

$$U_{top} = U_0 \left[\frac{1}{2}(\varphi_{top} - \varphi_x)^2 + \beta_L \cos\varphi_{top} \right]$$
$$\frac{\partial U_{top}}{\partial \varphi_x} = U_0 \left[\frac{\beta_L \sin\varphi_{top} - (\varphi_{top} - \varphi_x)}{\beta_L \cos(\varphi_{top}) - 1} - (\varphi_{top} - \varphi_x) \right]$$

From equations (28), (31) we obtain all other derivatives that should be found for calculation of the quantities $\alpha_{1,2}$, $\beta_{1,2}$.

$$\frac{\partial \lambda}{\partial E} = -\sqrt{\frac{2M}{U_1}} \tag{B.1}$$

$$\frac{\partial \lambda}{\partial \varphi_x} = U_0 \sqrt{\frac{2M}{U_1}} [\frac{1}{\beta_L \cos(\varphi_{top}) - 1} \left[\beta_L \sin\varphi_{top} \left(1 - \frac{U_{top} - E}{4U_1} \right) - (\varphi_{top} - \varphi_x) \right] - (\varphi_{top} - \varphi_x)] \tag{B.2}$$

$$\frac{\partial \chi}{\partial \lambda} = \frac{1}{2}\psi\left(\frac{1}{2}\right) + \lambda^2 \sum_{k=0}^{\infty} \frac{1}{(2k+1)((2k+1)^2 + \lambda^2)} \tag{B.3}$$

Now by using equations (45), (46), (B.1), (B.3) we obtain the value of all coefficients α_1, α_2, β_1, β_2.

$$\beta_1 = \frac{\partial \Phi_1}{\partial E} + \frac{1}{2}\frac{\partial \chi}{\partial \lambda}\frac{\partial \lambda}{\partial E} \tag{B.4}$$
$$= \sqrt{\frac{M}{2}} \int_{\tilde{\varphi}_1}^{\varphi_{top}} d\varphi \left(\frac{1}{\sqrt{U_{top} - U(\varphi)}} - \frac{\sqrt{\varphi_{top} - \tilde{\varphi}_1}}{(\varphi_{top} - \varphi)\sqrt{U_1(\varphi - \tilde{\varphi}_1)}} \right)$$
$$+ \sqrt{\frac{M}{2U_1}} \ln \left(\frac{8(MU_1)^{1/4}(\varphi_{top} - \tilde{\varphi}_1)}{2^{1/4}} \right) - \sqrt{\frac{M}{2U_1}} \frac{\partial \chi}{\partial \lambda}$$

$$\beta_2 = \frac{\partial \Phi_2}{\partial E} + \frac{1}{2}\frac{\partial \chi}{\partial \lambda}\frac{\partial \lambda}{\partial E} \tag{B.5}$$
$$= \sqrt{\frac{M}{2}} \int_{\varphi_{top}}^{\tilde{\varphi}_4} d\varphi \left(\frac{1}{\sqrt{U_{top} - U(\varphi)}} - \frac{\sqrt{\tilde{\varphi}_4 - \varphi_{top}}}{(\varphi - \varphi_{top})\sqrt{U_1(\tilde{\varphi}_4 - \varphi)}} \right)$$
$$+ \sqrt{\frac{M}{2U_1}} \ln \left(\frac{8(MU_1)^{1/4}(\tilde{\varphi}_4 - \varphi_{top})}{2^{1/4}} \right) - \sqrt{\frac{M}{2U_1}} \frac{\partial \chi}{\partial \lambda}$$

$$\alpha_1 = \frac{\partial \Phi_1}{\partial \varphi_x} + \frac{1}{2}\frac{\partial \chi}{\partial \lambda}\frac{\partial \lambda}{\partial \varphi_x} \tag{B.5}$$
$$= U_0\sqrt{\frac{M}{2}}\int\limits_{\varphi_1}^{\varphi_2} d\varphi \frac{\varphi - \varphi_x}{\sqrt{E - U(\varphi)}} + \left(\frac{1}{2}\frac{\partial \chi}{\partial \lambda} + \frac{1}{4}\ln\left(\frac{2}{\lambda}\right)\right) U_0\sqrt{\frac{2M}{U_1}}$$
$$\cdot[\frac{1}{\beta_L \cos\varphi_{top} - 1}\left[\beta_L \sin\varphi_{top}\left(1 - \frac{U_{top} - E}{4U_1}\right) - (\varphi_{top} - \varphi_x)\right]$$
$$-(\varphi_{top} - \varphi_x)]$$

$$\alpha_2 = \frac{\partial \Phi_2}{\partial \varphi_x} + \frac{1}{2}\frac{\partial \chi}{\partial \lambda}\frac{\partial \lambda}{\partial \varphi_x} \tag{B.6}$$
$$= U_0\sqrt{\frac{M}{2}}\int\limits_{\varphi_3}^{\varphi_4} d\varphi \frac{\varphi - \varphi_x}{\sqrt{E - U(\varphi)}} + \left(\frac{1}{2}\frac{\partial \chi}{\partial \lambda} + \frac{1}{4}\ln\left(\frac{2}{\lambda}\right)\right) U_0\sqrt{\frac{2M}{U_1}}$$
$$\cdot[\frac{1}{\beta_L \cos\varphi_{top} - 1}\left[\beta_L \sin\varphi_{top}\left(1 - \frac{U_{top} - E}{4U_1}\right) - (\varphi_{top} - \varphi_x)\right]$$
$$-(\varphi_{top} - \varphi_x)]$$

Appendix C

In the present appendix we give the transition matrix elements entering in the definition of $W_{f\,n}^{j\,m}$ (see Eq. (9) and Appendix A).

Transition matrix elements between states close to the barrier top can be calculated in quasiclassical approximation if the parameter λ (see Eq. (27)) is $\lambda \geq 1$. Consider first the matrix element $\langle L|\zeta|f_1\rangle$. With the help of Eqs. (27), (40), (41) we obtain

$$\langle L|\zeta|f_1\rangle = \frac{1}{G_L G_{E_{f_1}}}\int\limits_{\varphi_1(E_{f_1})}^{\varphi_2(E_{f_1})} d\varphi \frac{\sin\left(\pi/4 + \int\limits_{\varphi_1(E_L)}^{\varphi} d\varphi\sqrt{(2M\,(E_L - U(\varphi)))}\right)}{(2M\,(E_L - U(\varphi)))^{1/4}\,(2M\,(E_{f_1} - U(\varphi)))^{1/4}}\,\zeta \tag{C.1}$$
$$\sin\left(\pi/4 + \int\limits_{\varphi_1(E_{f_1})}^{\varphi} d\varphi\sqrt{(2M\,(E_{f_1} - U(\varphi)))}\right)$$

that is equal to

$$\langle L|\zeta|f_1\rangle = \frac{1}{2G_L G_{E_{f_1}}} \int \frac{d\varphi}{\sqrt{(2M\,(E_{f_1L} - U(\varphi)))}} \zeta \cos\left((E_{f_1} - E_L) \int_{\varphi_1(E_{f_1L})}^{\varphi} \frac{M d\varphi}{\sqrt{2M\,(E_{f_1L} - U(\varphi))}} \right) \tag{C.2}$$

To calculate the last integral we can use the time variable t according to the classical equation of motion

$$\frac{M}{2}\left(\frac{\partial\varphi}{\partial t}\right)^2 = E - U(\varphi) \tag{C.3}$$

As a consequence, Eq. (C.2) becomes

$$\langle L|\zeta|f_1\rangle = \frac{1}{2MG_L G_{E_{f_1}}} \int_0^{T_1/2} dt\zeta \cos\left(\frac{2\pi}{T_1} t\ell\right) \tag{C.4}$$

where T_1 is the period of the classical motion in the left potential well with energy E and ℓ is the number of states between energy levels E_{f_1} and E_L plus one. In our case $\ell = 1$. The initial value for φ is $\varphi(0) = \varphi_1$.

$$T_1 = 2M \int_{\varphi_1}^{\varphi_2} \frac{d\varphi}{\sqrt{(2M\,(E - U(\varphi)))}} \tag{C.5}$$

In the same way we obtain transition the matrix element $\langle R|\zeta|f_1\rangle$.

In Eq. (C.1) $\varphi_1(E_{f_1})$ is the first crossing point of the energy level E_{f_1} in the left well and $\varphi_2(E_{f_1})$ is the second crossing point of the energy level E_{f_1} in the left well.

In the same way in Eq. (C.2) $\varphi_1(E_{f_1L})$ is the first crossing point of the energy level E_{f_1L} in the left well, where E_{f_1L} is defined as

$$E_{f_1L} = \frac{E_{f_1} + E_L}{2} \tag{C.6}$$

Consider now the transition matrix element $\langle f_2|\ \zeta|f_1\rangle$. From Eq. (27) we find

$$\langle f_2|\ \zeta|f_1\rangle = \frac{\hbar}{2G_{f_1}G_{f_2}} \cdot \left[\int_{\varphi_1}^{\varphi_2} d\varphi \frac{\zeta}{\sqrt{(2M(E-U(\varphi)))}} + B_{f_1}B_{f_2} \int_{\varphi_3}^{\varphi_4} d\varphi \frac{\zeta}{\sqrt{(2M(E-U(\varphi)))}} \right] \tag{C.7}$$

where $\varphi_{1,2,3,4}$ are the turning points and E here is $E = \frac{\left(E_{f_1}+E_{f_2}\right)}{2}$. By using Eq. (C.3) we reduce the expression (C.7) to the form

$$\langle f_2|\ \zeta|f_1\rangle = \frac{\hbar}{2MG_{f_1}G_{f_2}} \left[\int_0^{T_1/2} dt\zeta + B_{f_1}B_{f_2} \int_0^{T_2/2} dt\zeta \right] \qquad \text{(C.8)}$$

In Eq. (C.8) the first integral is taken over the left potential well and the second one over the right potential well and T_1, T_2 are the periods of the classical motion in the left and in the right well respectively.

To improve Eq. (C.9) we should take into account ortogonality of wave-functions relative to the energies E_{f_1}, E_{f_2} . As result we obtain

$$\langle f_2|\ \zeta|f_1\rangle = \hbar\frac{1-B_{f_1}B_{f_2}}{2MG_{f_1}G_{f_2}} \left[\frac{T_2}{T_1+T_2} \int_0^{T_1/2} dt\zeta - \frac{T_1}{T_1+T_2} \int_0^{T_2/2} dt\zeta \right] \qquad \text{(C.9)}$$

The research of one of us (Yu.N.O.) is supported by Cariplo Foundation-Italy, CRDF USA under Grant No. RP1-2565-MO-03 and the Russian Foundation of Basic Research. This work has been partially supported by MIUR under Project “Reti di Giunzioni Josephson per la Computazione e l’Informazione Quantistica-JOSNET".

References

[1] A.O. Caldeira and A.J. Leggett, Phys. Rev. Lett. **46**, 211 (1981).

[2] D.B. Schwartz, B. Sen, C.N. Archie, and J.E. Lukens, Phys. Rev. Lett. **55**, 1547 (1985).

[3] S. Washburn, R.A. Webb, R.F. Voss, and S.M. Faris, Phys. Rev. Lett. **54**, 2712 (1985).

[4] R. Rouse, S. Han, and J.E. Lukens, Phys. Rev. Lett. **75**, 1614 (1995).

[5] J.M. Martinis, M.H. Devoret, and J. Clarke, Phys. Rev. Lett. **55**, 1543 (1985).

[6] J.M. Martinis, M.H. Devoret, and J. Clarke, Phys. Rev. B **35**, 4682 (1987).

[7] P. Silvestrini, V.G. Palmieri, B. Ruggiero, and M. Russo, Phys. Rev. Lett. **79**, 3046 (1997).

[8] J.R. Friedman, V. Patel, W. Chen, S.K. Tolpygo, and J.E. Lukens, Nature (London) **406**, 43 (2000).

[9] I. Chiorescu, Y. Nakamura, C.J.P.M. Harmans, and J.E. Mooij, Science **299**, 1036 (2003).

[10] J. Claudon, F. Balestro, F.W.J. Hekking, and O. Buisson, Phys. Rev. Lett. **93**, 187003 (2004).

[11] M.H. Devoret and J.M. Martinis, *Quantum Entanglement and Information Processing* - Les Houches Summer School Proceedings **79**, Ed.: D. Esteve, J.M. Raimond, and J. Dalibard (Elsevier, San Diego, CA, 2004).

[12] A.I. Larkin and Yu.N. Ovchinnikov, J. of Low Temp. Phys. **63**, 317 (1986).

[13] Yu.N. Ovchinnikov and A. Schmid, Phys. Rev. B **50**, 6332 (1994).

[14] D. Averin, J. Low Temp. Phys. **118**, 781 (2000).

[15] D.V. Averin, J.R. Friedman, and J.E. Lukens, Phys. Rev. B **62**, 11802 (2000).

[16] A.I. Larkin and Yu.N. Ovchinnikov, Sov. Phys. JETP **64**, 185 (1986).

[17] U. Fano, Rev. of Mod. Phys. **29**, 74 (1957).

[18] A. Barone and G. Paternó, *Physics and Applications of the Josephson Effect* (Wiley, New York, 1982).

[19] R. Cristiano, L. Frunzio, C. Nappi, M.G. Castellano, G. Torrioli, and C. Cosmelli, J. Appl. Phys. **81**, 7418 (1997).

[20] U. Eckern, G. Schon, and V. Ambegaokar, Phys. Rev. B **30**, 6419 (1984).

[21] Y.C. Chen, M.P.A. Fisher, and A.J. Leggett, J. Appl. Phys. **64**, 3119 (1988).

[22] A.I. Larkin and Yu.N. Ovchinnikov, Phys. Rev. B **28**, 6281 (1983).

[23] A.I. Larkin and Yu.N. Ovchinnikov, Sov. Phys. JETP **60**, 1060 (1984).

[24] I.M. Ryzhik and I.S. Gradstein, *Table of Integrals, Series and Products*, (Academic Press, New York, 1965).

[25] L. Landau and L. Lifshitz, *Quantum Mechanics: non-relativistic theory*, vol.3 (Butterworth-Heinemann, 1981).

[26] Yu.N. Ovchinnikov, P. Silvestrini, V. Corato, and S. Rombetto, Phys. Rev. B **71**, 024529 (2005).

[27] P. Silvestrini, B. Ruggiero, and Yu.N. Ovchinnikov, Phys. Rev. B **54**, 1246 (1996).

[28] M.H. Devoret, J.M. Martinis, D. Esteve, and J. Clarke, Phys. Rev. Lett. **53**, 1260 (1984).

[29] M.H. Devoret, J.M. Martinis, and J. Clarke, Phys. Rev. Lett. **55**, 1543 (1985).

[30] A.I. Larkin and Yu.N. Ovchinnikov, JETP Letters **39**, 681 (1984).

[31] A.I. Larkin and Yu.N. Ovchinnikov, *Quantum Tunnelling in condensed media* Ed.: Yu.N. Ovchinnikov and A.J. Legget (Elsevier, 1992).

[32] D. Averin, Solid State Commun. **105**, 659 (1998).

[33] V. Corato, S. Rombetto, C. Granata, E. Esposito, L. Longobardi, M. Russo, R. Russo, B. Ruggiero, and P. Silvestrini, Phys. Rev. B **70**, 172502 (2004).

[34] C.H. van der Wal, A.C.J. Ter Haar, F.K. Wilhem, R.N. Schouten, J.P.M. Harmaas, T.P. Orlando, S. Lloyd, and J.E. Mooij, Science **285**, 1036 (2000).

[35] J.B. Majer, F.G. Paauw, A.C.J. ter Haar, C.J.P.M. Harmans , and J.E. Mooij, Phys. Rev. Lett. **94**, 090501 (2005).

[36] N. Groenbech-Jensen and M. Cirillo, Phys. Rev. B **70**, 214507 (2004).

[37] D. Averin, Solid State Commun. **105**, 659 (1998).

[38] R. Rouse, S. Han, and J.E. Lukens, Phys. Rev. Lett. **79**, 3036 (1997).